Report

Neuron

Conversion of Graded Presynaptic Climbing Fiber Activity into Graded Postsynaptic Ca^{2+} Signals by Purkinje Cell Dendrites

Highlights

- Individual climbing fibers are responsive to multiple sensory modalities
- Sensory-evoked Ca^{2+} events in climbing fibers are larger than spontaneous events
- Silencing olivary neurons abolishes Purkinje cell dendritic Ca^{2+} activity
- Purkinje cell dendrites faithfully integrate the level of climbing fiber activity

Authors

Michael A. Gaffield, Audrey Bonnan, Jason M. Christie

Correspondence

jason.christie@mpfi.org

In Brief

Gaffield et al. find that sensory stimuli enhance climbing fiber responsiveness, leading to larger Purkinje cell Ca^{2+} events. This integrative process is unaffected by local neural circuits, indicating the primacy of the inferior olive in instructional signaling.

Gaffield et al., 2019, Neuron *102*, 762–769
May 22, 2019
https://doi.org/10.1016/j.neuron.2019.03.010

CellPress

CellPress

Neuron
Report

Conversion of Graded Presynaptic Climbing Fiber Activity into Graded Postsynaptic Ca^{2+} Signals by Purkinje Cell Dendrites

Michael A. Gaffield,[1] Audrey Bonnan,[1] and Jason M. Christie[1,2,*]
[1]Max Planck Florida Institute for Neuroscience, Jupiter, FL, USA
[2]Lead Contact
*Correspondence: jason.christie@mpfi.org
https://doi.org/10.1016/j.neuron.2019.03.010

SUMMARY

The brain must make sense of external stimuli to generate relevant behavior. We used a combination of *in vivo* approaches to investigate how the cerebellum processes sensory-related information. We found that the inferior olive encodes contexts of sensory-associated external cues in a graded manner, apparent in the presynaptic activity of their axonal projections (climbing fibers) in the cerebellar cortex. Individual climbing fibers were broadly responsive to different sensory modalities but relayed sensory-related information to the cortex in a lobule-dependent manner. Purkinje cell dendrites faithfully transformed this climbing fiber activity into dendrite-wide Ca^{2+} signals without a direct contribution from the mossy fiber pathway. These results demonstrate that the size of climbing-fiber-evoked Ca^{2+} signals in Purkinje cell dendrites is largely determined by the firing level of climbing fibers. This coding scheme emphasizes the overwhelming role of the inferior olive in generating salient signals useful for instructing plasticity and learning.

INTRODUCTION

The cerebellum is thought to use sensory prediction errors to guide learning by plastic alteration of its circuitry. Climbing fibers (CFs) that arise from the inferior olive are well suited to transmit sensory prediction errors to Purkinje cells (PCs), the sole output neurons of the cerebellar cortex. This is because each CF stimulation reliably initiates both a PC somatic complex spike and a dendrite-wide burst of Ca^{2+} action potentials (Llinás and Sugimori, 1980). PCs encode descriptive information regarding sensory prediction errors by interpreting the population dynamics of these CF inputs (Brown and Raman, 2018; Herzfeld et al., 2018) and the variance of evoked somatic and dendritic responses that distinguish behaviorally relevant CF events from spontaneous activity (Kitamura and Häusser, 2011; Najafi et al., 2014a, 2014b; Yang and Lisberger, 2014). Such variability in discrete CF-evoked Ca^{2+} events may promote efficient coding of Ca^{2+}-induced plasticity and learning in PC dendrites (Najafi and Medina, 2013; Rowan et al., 2018). However, the neural circuit mechanisms that support graded coding of CF-mediated signals are not fully resolved.

Olivary projection neurons fire bursts of spikes whose duration is influenced by the intrinsic dynamics of subthreshold oscillatory activity (Crill, 1970; De Gruijl et al., 2012; Leznik and Llinás, 2005). Therefore, the inferior olive is poised to directly convey processed information pertaining to external cues to the cerebellar cortex through variable-duration CF burst firing, particularly if their activity is subject to sensory amplification (Maruta et al., 2007). Yet, mossy fibers also relay sensorimotor information to PCs by way of granule cells. Through direct excitation and feedforward inhibition, granule cell activity can contribute to and/or modulate the CF-mediated dendritic Ca^{2+} response (Callaway et al., 1995; Wang et al., 2000).

In this study, we examined how PC dendrites process sensory-related information in the lateral cerebellum using a combination of *in vivo* Ca^{2+} imaging and genetically encoded effectors of activity. We report that individual PC dendrites are reliably responsive to different modalities of sensory stimuli and remarkably sensitive to the presynaptic activity level of CFs. The absence of any additional, residual Ca^{2+} response from non-olivary inputs supports the conclusion that PCs faithfully convert sensory-enhanced CF excitation into graded, dendrite-wide Ca^{2+} signals. Thus, CFs provide near-exclusive sources of the instructive signals thought to be necessary for plasticity and learning in the cerebellum.

RESULTS

Sensory Stimuli Trigger Enhanced Ca^{2+} Signals in PC Dendrites

We used two-photon laser scanning microscopy (2pLSM) to measure Ca^{2+} signals in the dendrites of GCaMP6f-expressing PCs located in the lateral posterior cerebellum of awake, head-fixed mice (Figure 1A). Dendritic spikes, attributable to the activity of presynaptic CFs, were resolved as rapidly rising Ca^{2+} events (Ozden et al., 2008; Schultz et al., 2009); their continuous occurrence reflecting the regular, spontaneous output of the inferior olive (1.01 ± 0.05 Hz). We used a variety of sensory stimuli to activate the cerebellum and look for evoked responses in PCs (Figure 1B). For this, we used somatosensory (air puff to the

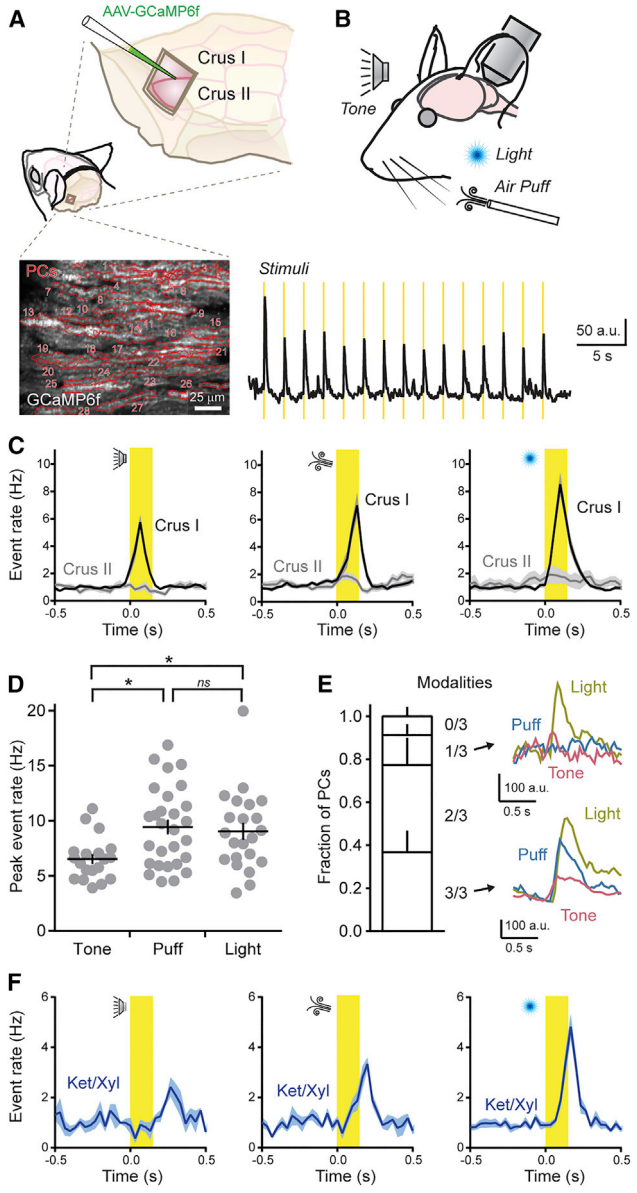

Figure 1. PCs in Crus I Are Broadly Responsive to Different Sensory Modalities

(A) Cranial windows were positioned over the left lateral cerebellum where PCs expressed GCaMP6f as shown in the fluorescence image below. Red lines demarcate the dendritic contours of individual PCs (n = 28).

(B) Top: sensory stimuli were presented to mice while measuring neural activity. Bottom: average ensemble Ca^{2+} response across PC dendrites (n = 20 trial blocks). Stimulus timing is shown in yellow.

(C) Trial-averaged dendritic Ca^{2+} event rates for each sensory modality (i.e., tone, puff, light) across all PCs, compiled from measurements obtained from two different cerebellar lobules (n = 5–28 trial blocks from 6–10 mice per condition).

(D) The peak rate of evoked Ca^{2+} events in Crus I PCs for each sensory modality across awake mice (each dot represents the average of a block of stimulus trials; 6–10 mice for each condition). Data are mean ± SEM with p = 0.01 for tone-puff comparison, p = 0.04 for tone-light comparison, and p = 0.90 for puff-light comparison; ANOVA with Tukey's multiple comparison test.

(E) Left: fraction of identified PCs in Crus I, categorized based on their responsiveness to presentation of different sensory modalities (n = 141 cells from 3 mice). Right: average dendritic Ca^{2+} transients from two different PCs that were either selectively (top) or broadly (bottom) responsive to modality types.

(F) Dendritic Ca^{2+} event rates, measured in Crus I PCs, in response to sensory stimuli while the animal was under anesthesia (n = 3–9 trial blocks; 2–4 mice per condition).

See also Figure S1.

ipsilateral whiskers [18 psi; 150 ms]), auditory (12 kHz tone; ~85 dB; 150 ms), and visual (light flash directed to the ipsilateral eye [λ = 473 nm; 25 μW; 150 ms]) stimuli. We presented each sensory modality in a block of 15 closely spaced trials (0.5 Hz), randomly switching between stimulus types from one block to the next to prevent habituation.

In lobule Crus I, each sensory modality reliably triggered dendritic spiking across the PC ensemble that was time-locked to the presentation of individual stimuli (Figure 1C). We found slight differences in peak rates of sensory-triggered Ca^{2+} events across modalities (Figure 1D). The vast majority of individual PCs within ensembles responded to more than one modality (Figure 1E). This result suggests that CFs in Crus I generally report the occurrence of an external stimulus rather than encode modality type. Simultaneously presenting two modalities had a non-additive effect on the rate of CF-evoked events, indicating that ensemble responsiveness to multiple stimulus types was near saturation (Figures S1A and S1B).

Interestingly, there was evidence of partitioned processing of different types of behaviorally relevant information in distinct regions of the lateral cerebellum. In lobule Crus II, where PCs are responsive to motor-related CF activity (Gaffield et al., 2016; Gaffield and Christie, 2017), sensory cues failed to alter the rate of dendritic Ca^{2+} events compared to baseline (1.22 ± 0.12 and 1.20 ± 0.14 Hz; prior to and during sensory stimuli, respectively; n = 39 trial blocks, 6 mice; p = 0.93; paired Student's t test; Figure 1C). Given that sensory-triggered Ca^{2+} events persisted in PCs of Crus I while animals were under anesthesia-induced paralysis, in particular to auditory and visual stimuli, we rule out movement as the direct cause of CF responses in this region (Figure 1F). These results emphasize the modular organization of divergent input streams into the cerebellar cortex.

Examining isolated CF-evoked Ca^{2+} events in Crus I PC dendrites (see STAR Methods) revealed that responses resulting from sensory stimuli were distinguishable from spontaneous activity based on the responses' enhanced size (peak integral 27.5% ± 3.2% larger on average; n = 74 trial blocks, 12 mice; p < 0.001; paired Student's t test). This result was consistent across modalities (Figure 2A). The amount of enhancement varied slightly with stimulus type (Figure 2B), which is in line with previous reports of graded coding of sensory-evoked CF activity by PC dendrites (Najafi et al., 2014a, 2014b). However, the subtle differences in sensory enhancement between modality types suggest that stimuli produce near-saturating responses. This also indicates a limited bandwidth within which graded enhancement can be encoded. In summary, lobule-specific CFs broadly encode the occurrence of external sensory cues

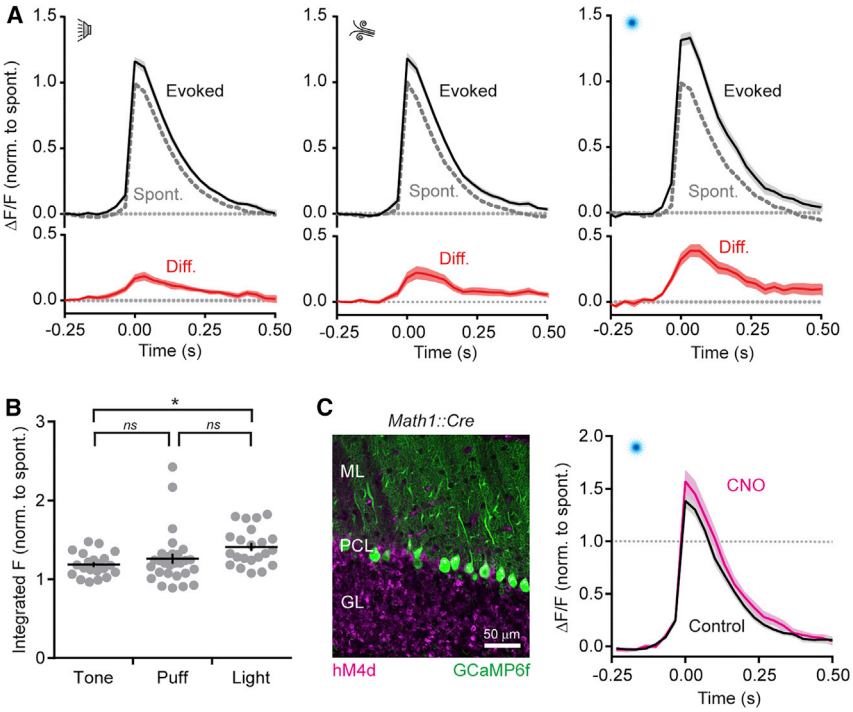

Figure 2. Graded Coding of Sensory-Related Ca^{2+} Events in PC Dendrites

(A) Average isolated dendritic Ca^{2+} events, collected across Crus I PC dendrites from all mice, during presentation of sensory stimuli. Peak amplitudes are normalized to that of spontaneous events with the difference plotted in red below.

(B) The peak amplitude of the integral for average, sensory-associated Ca^{2+} events, relative to that of spontaneous responses, for each block of stimulus trials (indicated by gray dots). Data are mean ± SEM; *p = 0.02, ns, not significant, p = 0.59 and 0.12; ANOVA with Tukey's multiple comparison test (n = 21–28 trial blocks; 6–10 mice per condition).

(C) Left: image of hM4d-expressing granule cells and GCaMP6f-expressing PCs. Right: average isolated dendritic Ca^{2+} events in PCs during sensory cue presentation (light flash), normalized to that of spontaneous responses. Measurements obtained from the same regions of Crus I in control and after CNO administration (n = 9 regions from 3 mice).

See also Figures S2–S4.

across modalities, generating graded Ca^{2+} signals in PC dendrites that are larger than spontaneous events.

Inhibition Does Not Account for Differences in CF-Evoked Dendritic Ca^{2+} Signaling

Inhibition from molecular layer interneurons (MLIs) can influence the integrated PC response to CF excitation, reducing the amplitude of dendritic Ca^{2+} signals (Callaway et al., 1995; Kitamura and Häusser, 2011). However, we observed little spontaneous Ca^{2+} activity in RCaMP2-expressing MLIs as animals sat in quiescence (Figures S2A and 2B). To examine for the co-occurrence of MLI activity with spontaneous CF-evoked responses in PCs at high temporal resolution, we averaged dendritic events in GCaMP6f-expressing PCs and the simultaneously measured, corresponding Ca^{2+} signals in surrounding RCaMP2-expressing MLIs (Figures S2B and 2C). The lack of a coincident increase in MLI Ca^{2+} activity, time-locked to the PC response, indicates that inhibition does not suppress the size of spontaneous dendritic Ca^{2+} events in PCs and, therefore, cannot account for size disparities in CF-mediated Ca^{2+} signaling during behaviorally relevant contexts.

In contrast to their basal activity level, MLIs in Crus I were highly responsive to sensory stimuli, with each modality generating robust and widespread activation of their ensemble (Figures S3A and 3B). To determine whether parallel fiber excitation contributes to sensory-induced MLI activity, we transduced granule cells with hM4d, a chemogenetic inhibitor (Armbruster et al., 2007), and measured Ca^{2+} activity in MLIs expressing GCaMP6f (Figure S3C). The reduction in sensory-evoked MLI activity after intraparietal injection of the hM4d agonist clozapine-N-oxide (CNO; Figures S3D and 3E) supports the conclusion that the mossy fiber pathway also conveys sensory-related information into the cerebellar cortex, relaying this information to the molecular layer by way of granule cells. Notably, sensory-enhanced PC Ca^{2+} signaling occurred despite the coincident activation of CFs and MLIs during cue presentation, as measured by dual-color Ca^{2+} sensor imaging in non-hM4d-expressing animals (Figure S4A). Surprisingly, the trials that produced the largest changes in PC Ca^{2+} event size were correlated with the greatest levels of MLI activation (Figure S4B). An inverse relationship would be expected if MLI-mediated inhibition was directly responsible for producing variable amplitude CF-evoked Ca^{2+} events during cue presentation. Therefore, PC dendrites must integrate activity from a neural source other than that of MLIs to affect the size of sensory-enhanced CF responses.

Lack of Residual Dendrite-wide Ca^{2+} Signaling in the Absence of CF Activity

Parallel-fiber-mediated excitation of PC dendrites can induce intracellular Ca^{2+} elevation through electrogenic and second-messenger pathways (Ly et al., 2016; Rancz and Häusser, 2006; Tempia et al., 2001). Granule cell activity, driven by sensorimotor stimuli (Chadderton et al., 2004; Chen et al., 2017), could thus directly contribute to the sensory-evoked enhancement of Ca^{2+} signaling in PCs (Najafi et al., 2014b). However, chemogenetic-induced activity suppression of hM4d-expressing granule cells had no effect on the size of isolated, sensory-related Ca^{2+} responses in GCaMP6-expressing PCs (p = 0.18, Student's t test, Figure 2C). Nor did it alter the overall rate of evoked dendritic events (peak control rate = 8.62 ± 0.80 Hz, peak CNO rate = 7.71 ± 0.69 Hz, p = 0.39, Student's t test, n = 9 regions, 3 mice). Though this result argues against the direct contribution of granule cells to sensory enhancement of PC dendritic Ca^{2+} signaling, our approach likely produces only a partial reduction in output from the granule cell ensemble (see Figures S3D and 3E). Therefore, we also looked for residual, dendrite-wide Ca^{2+}

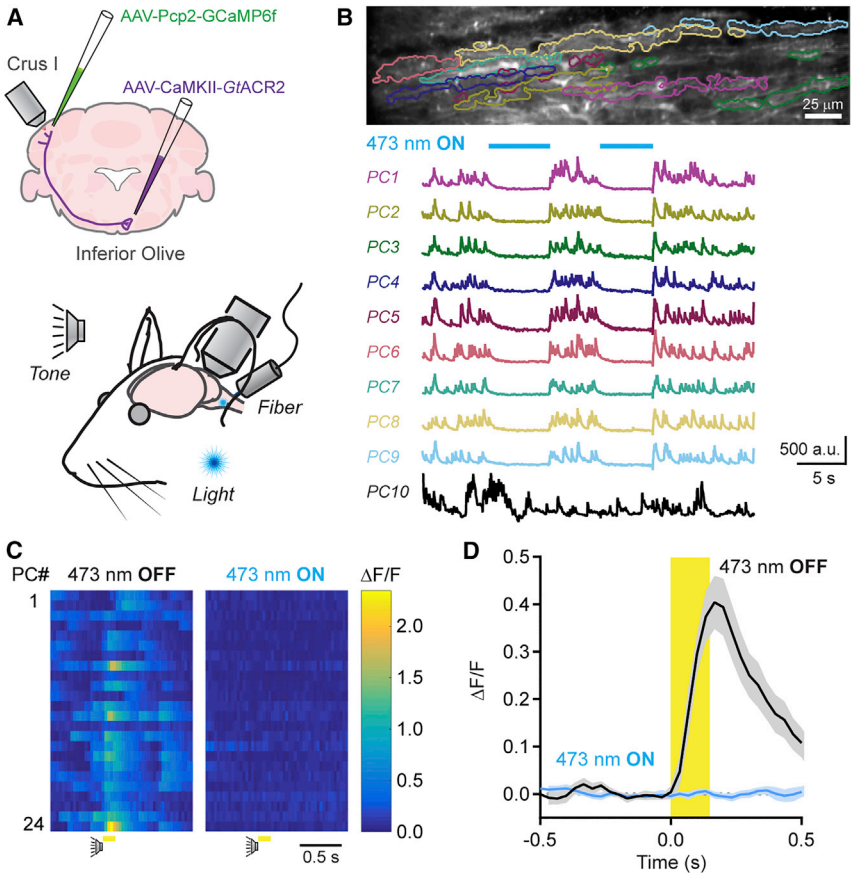

Figure 3. Dendrite-wide Ca^{2+} Signals in PCs Are Completely Mediated by CFs

(A) *Gt*ACR2 was expressed in excitatory neurons of the inferior olive; dendritic Ca^{2+} activity was measured in GCaMP6f-expressing PCs of Crus I during sensory stimuli. Sensory cues were presented to the animal, while in a subset of trials, an optical fiber implant continuously delivered laser light to the inferior olive.

(B) Spontaneous Ca^{2+} activity in PCs, demarcated in the fluorescence image above, was abolished during photo-illumination of the inferior olive ($\lambda = 473$; 250 μW). An example PC (PC10) is included that was persistently active during the optogenetic stimulus.

(C) Ca^{2+} activity measurements for individual PCs in a field of view in response to an auditory stimulus in control or during the continuous optogenetic suppression of the inferior olive ($\lambda = 473$; 250 μW).

(D) Average Ca^{2+} activity transients across PC dendrites to sensory stimuli (including both auditory and visual cues) in control and with optogenetic suppression of the inferior olive. Data are mean ± SEM (n = 234 cells from 4 mice; 10 trial blocks for each condition).

See also Figures S5–S7.

signals in PCs that may be attributable to parallel fibers by suppressing CF activity during sensory cue presentation.

For this approach, we expressed the inhibitory anion-fluxing channelrhodopsin variant *Gt*ACR2 (Govorunova et al., 2015) in excitatory olivary neurons. Using an implanted optical fiber that targeted the inferior olive, we photoinhibited *Gt*ACR2-expressing cells and imaged Ca^{2+} activity in GCaMP6f-expressing Crus I PCs (Figure 3A). During awake quiescence, the frequency of spontaneous dendritic Ca^{2+} events was markedly reduced during the illumination period (1.15 ± 0.21 and 0.21 ± 0.08 Hz; control and with photoinhibition, respectively; n = 10 epochs, 4 mice; p = 0.005, Student's t test) and returned to baseline levels after cessation of the optogenetic stimulus (1.30 ± 0.20 Hz). Further analysis revealed that a subset of PCs, comprising 47.9% ± 4.2% of their population, was significantly affected by optogenetic suppression of the inferior olive. In these cells, spontaneous Ca^{2+} activity was essentially absent during the photo-stimulus (Figure 3B). In separate sessions, extracellular electrophysiological measurements of PC units in these same mice during illumination of the inferior olive revealed the complete elimination of complex spikes without disruption to simple spiking (Figures S5A–S5C). The remaining PC population showed normal levels of spontaneous activity during optogenetic suppression, likely due to incomplete transduction of all olivary projection neurons. Together, these results confirm that CFs drive spontaneous dendritic Ca^{2+} events in PCs.

Among PCs that were sensitive to spontaneous activity suppression, optogenetic inhibition of the inferior olive also affected their Ca^{2+} responses to sensory stimulation. When presented with external cues during the continuous photo-suppression of the inferior olive, there was an absence of algorithmically identifiable dendritic Ca^{2+} events within the cue window (1.9% ± 1.3% of control rate; p = 0.002; n = 10 trials, 4 mice; paired Student's t test; Figure 3C). Furthermore, in trial-averaged responses aligned to the timing of the sensory stimulus, there was a lack of resolvable dendrite-wide Ca^{2+} signal in PCs during cue presentation (Figure 3D). Likewise, simply removing algorithmically identified Ca^{2+} events in PCs from a subset of curated trials in control mice produced a qualitatively similar result (Figure S6). Photo-illumination of the inferior olive had no effect on sensory enhancement of CF-evoked Ca^{2+} signals among neighboring PCs that were insensitive to spontaneous activity suppression (Figures S7A and S7B), ruling out a spurious result owing to off-target expression of *Gt*ACR2 in mossy fiber projection neurons in the brainstem. Together, these results indicate that CF activity fully accounts for the sensory enhancement of Ca^{2+} responses in PC dendrites.

Sensory Enhancement Is Encoded in the Presynaptic Activity Level of CFs

If conveyed to the cerebellar cortex by CF axons, burst firing in olivary projection neurons (Crill, 1970) could generate graded levels of excitation in postsynaptic PCs dependent on the number of action potentials in the presynaptic burst (Mathy et al., 2009). In fact, *ex vivo* recording of CF-evoked Ca^{2+} activity in PC dendrites revealed that response amplitude increased with

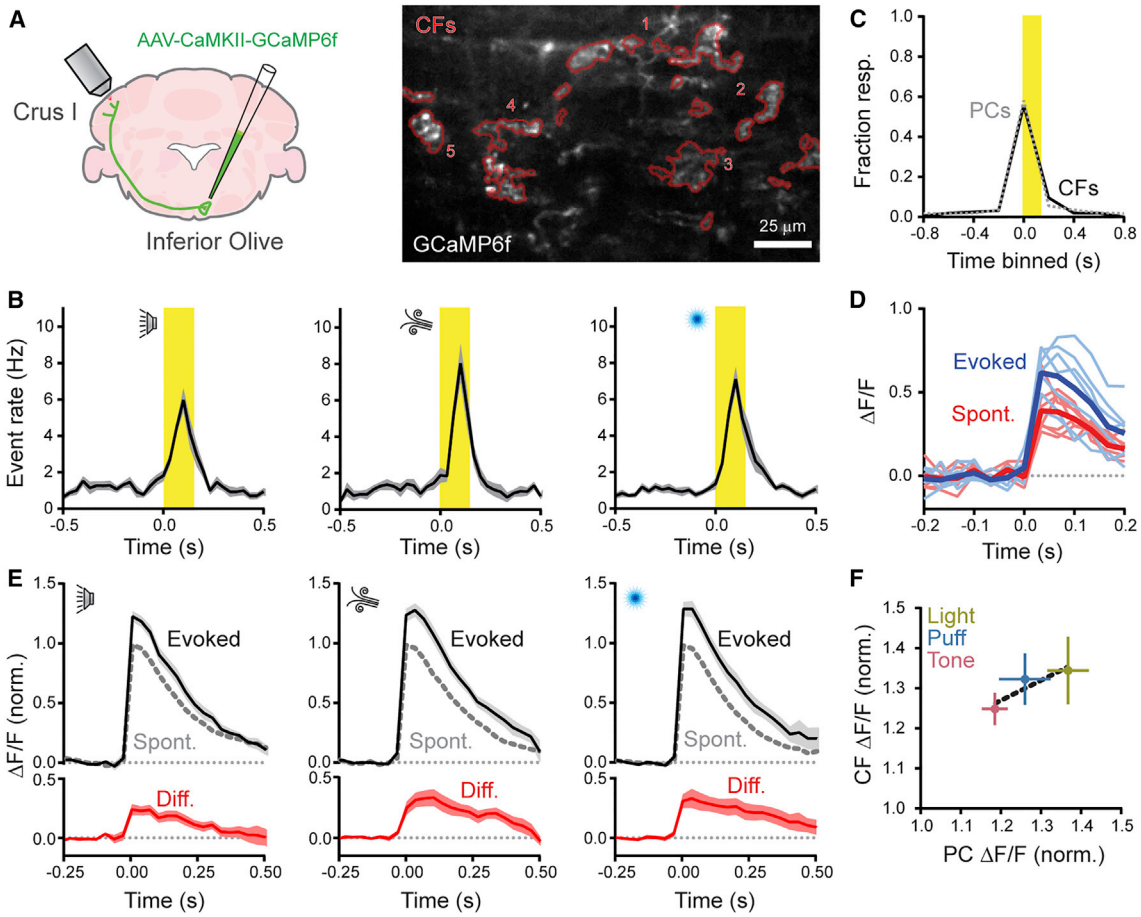

Figure 4. Sensory Enhancement of Presynaptic Ca^{2+} Events in CFs

(A) Viral infection of the right inferior olive drove GCaMP6f expression in CFs innervating left Crus I. In the fluorescence image, contours of GCaMP6f-expressing CFs (n = 5) are in red.

(B) Plots of Ca^{2+} event rates in CFs, evoked by different sensory modalities. Stimulus timing in yellow (n = 12–15 trial blocks; 5 mice per condition).

(C) Fraction of sensory-responsive CFs was similar to that of PCs. Measurements were obtained from separate cohorts of animals (n = 613 PCs and 79 CFs; 5 and 10 mice, respectively).

(D) Isolated Ca^{2+} events, collected from a single CF, were categorized by whether they occurred spontaneously or in response to the sensory stimulus (thick lines are means).

(E) Average spontaneous and sensory-evoked Ca^{2+} events across CFs for different sensory modalities; the difference is shown in red (n = 13–16 trial blocks, 5 mice).

(F) Comparison of the sensory enhancement of Ca^{2+} event amplitudes in CFs and observations in PCs, measured in separate experiments. The change in PC response size closely parallels that of CFs across modalities. Data are mean ± SEM.

See also Figure S8.

the number of spikes in a high-frequency burst of presynaptic stimuli (Figures S8A and 8B). Therefore, sensory enhancement of CF burst duration could contribute to larger dendritic Ca^{2+} responses in awake mice.

To directly measure CF activity *in vivo*, we virally transduced olivary projection neurons with GCaMP6f to express this indicator in their axons (Figure 4A). We readily observed spontaneous Ca^{2+} events in Crus I CFs with an event frequency that closely matched the rate of Ca^{2+} events in PC dendrites, as measured in separate mice (1.04 and 1.01 Hz, respectively; n = 5 and 12 mice; p = 0.75; Student's t test). CFs were also activated in response to sensory stimuli with evoked Ca^{2+} event rates that were comparable to the rates observed in PC dendrites (Figure 4B). The fraction of sensory-responsive CFs was identical to that of PCs (Figure 4C). These results strongly suggest that CFs reliably excite PCs *in vivo*.

Next, we examined the size of isolated Ca^{2+} events in CFs and found that responses during sensory cue presentation were larger than responses that occurred outside of the stimulus window (Figure 4D). Thus, on average, sensory stimuli produced an enhancement of presynaptic signaling (peak integral 30.9% ± 3.9% larger than spontaneous events; n = 38 trial blocks; 5 mice; $p < 0.001$; paired Student's t test). This result held true across sensory modalities (Figure 4E). There was a strong correlation between sensory-induced enhancement of CF Ca^{2+} event size and the induced increase measured in PC dendrites for each

stimulus type (R^2 = 0.84; Figure 4F). In conclusion, the presynaptic activity level of CFs changes in response to sensory stimuli, transferring information in a graded manner, at high fidelity, from the inferior olive to PCs producing variably sized dendritic Ca^{2+} responses.

DISCUSSION

PC Dendrites Broadly Encode the Occurrence of Sensory Stimuli across Modalities

CF inputs map a fractured somatotopy onto the cerebellar cortex, producing zones of like-responding PCs to sensorimotor stimuli (Apps and Hawkes, 2009). Here, we report lobule-specific responsiveness of PCs to CF-mediated excitation, with sensory stimuli reliably driving activation of PCs in Crus I, but not Crus II. CF responses in Crus I were not due to motor action as sensory-related activity persisted under anesthesia-induced paralysis. In previous studies, we also observed lobule-specific differences in the representation of behavioral variables, with orofacial movements in response to reward consumption engaging neurons in Crus II, but not Crus I (Gaffield et al., 2016; Gaffield and Christie, 2017). Combined, these results suggest partitioned representations of unpredicted sensations and mechanics of action within the lateral posterior hemispheres. Interestingly, we found that individual PCs in Crus I were broadly responsive to multiple sensory modalities. The general lack of CF tuning argues that olivary neurons report the occurrence of a cue rather than a particular sensory event type. This may be conducive for encoding associations to any unexpected external event encountered in the environment and its repercussions to the animal's behavior.

PC Dendrites Integrate the Level of Presynaptic CF Activity

The integrative properties of PC dendrites allow for a large repertoire of CF-mediated responses beyond that of "all-or-none" excitation (Najafi and Medina, 2013). A major finding of our work is that PCs are sensitive to the activity level of CFs, generating graded dendritic Ca^{2+} signals that, on average, change in proportion to size alterations of evoked, presynaptic Ca^{2+} responses. Importantly, size-enhanced CF-evoked signals occurred in response to external cues. This indicates that behaviorally relevant stimuli, such as an unexpected sensory cue, can be differentially encoded by CFs, perhaps adding to the saliency of these cues. Because olivary neurons fire variable-duration bursts of action potentials that are transmitted along their axon (Crill, 1970; Mathy et al., 2009), we surmise that presynaptic Ca^{2+} events in CFs correspond to discrete bursts. Therefore, the size of these presynaptic Ca^{2+} events reports burst duration (i.e., the number of spikes in the burst) rather than the number of discrete bursts.

Our *ex vivo* results indicate that even small shifts in presynaptic burst duration, including one or two additional spikes in the CF burst, are distinguishable in the evoked PC dendritic Ca^{2+} response and may account for sensory enhancement *in vivo*. PC dendrites are capable of continuously integrating many CF stimuli. Therefore, saturation of sensory-enhanced Ca^{2+} signaling in awake mice is apt to reflect a restricted range of CF burst firing during behavior. The spike content of olivary bursts changes with the amplitude and phase of subthreshold oscillatory activity in these neurons (Chorev et al., 2007; Leznik and Llinás, 2005). Network coherence and phase-resetting of subthreshold oscillations in olivary neuron ensembles (De Gruijl et al., 2012; Khosrovani et al., 2007) may be influenced by sensory stimuli, promoting amplification of burst duration when animals are confronted with unexpected cues. We suspect there is a limit to which these processes promote increased olivary firing, setting a narrow bandwidth for graded signaling during sensory cues. Yet, any sensory amplification of olivary output would be relayed to PCs by CFs and, based on our observations, linearly transformed into dendritic Ca^{2+} signals through locally generated electrogenic potentials (Davie et al., 2008; Otsu et al., 2014).

Dendritic-wide Ca^{2+} Signaling in PC Dendrites Is Exclusively Mediated by the Activity of CFs

In addition to CF-mediated input, PC dendrites integrate excitation and inhibition from parallel fibers and MLIs, respectively, whose activity can modulate the size of CF-evoked Ca^{2+} responses. However, differences in the size of spontaneous and sensory-related, dendrite-wide Ca^{2+} events are probably not attributable to the direct activity of either of these inputs for three reasons. First, MLIs appeared to be relatively inactive during quiescence, suggesting that inhibition of CF-evoked dendritic Ca^{2+} signaling in PCs does not account for the reduced size of spontaneous events. In fact, in Crus II, chemogenetic disinhibition of the molecular layer has no effect on spontaneous Ca^{2+} event amplitudes (Gaffield et al., 2018). Interestingly, we observed that MLIs in Crus I were co-activated with PCs in response to sensory cue presentation. Thus, although inhibitory output increased, CFs were still able to drive larger dendritic Ca^{2+} events in this behavioral context. Second, chemogenetic suppression of granule cell activity failed to affect sensory-induced enhancement of PC Ca^{2+} event size. Third, we failed to observe residual Ca^{2+} signals in PC dendrites in response to sensory stimulation when the output of the inferior olive was optogenetically suppressed. If sensory-evoked parallel fiber activity directly triggered a dendrite-wide Ca^{2+} signal (Najafi et al., 2014b), then this should have been revealed in this condition.

Our results do not rule out possible roles for these modulatory inputs in graded coding of behaviorally relevant PC Ca^{2+} signals. For example, the coincident activity of parallel fibers can produce an indirect, non-linear enhancement of CF-evoked responses, apart from direct Ca^{2+} entry, by affecting PC dendritic excitability (Otsu et al., 2014; Wang et al., 2000). However, this non-linear enhancement is tightly regulated by feedforward inhibition (Gaffield et al., 2018), and any behavioral contexts that enable granule cells to influence CF-evoked responses have yet to be identified. It is also possible that parallel fibers and/or MLIs have a subcellular influence on PC dendritic Ca^{2+} signaling (Roome and Kuhn, 2018), not apparent in the average, arbor-wide response. We hypothesize that sensory enhancement of CF burst firing may aid in the efficacy of learning (Najafi and Medina, 2013). By generating a corresponding increase in the size of PC dendritic Ca^{2+} signals, longer duration CF bursts can help determine the direction and strength of short- and long-term synaptic plasticity at parallel fiber inputs (Coesmans et al., 2004; Mathy et al., 2009). The direction of CF-induced

plasticity will depend on a number of factors, including the previous history of plasticity across all PC synapses, and the relative, rather than absolute, increase in dendritic Ca^{2+} (Hansel and Linden, 2000; Piochon et al., 2016). In the absence of a dendrite-wide modulatory influence through the mossy fiber pathway, information is transferred from CFs to PCs at high fidelity, ensuring a reliable coding scheme whereby instructive signals for plasticity and learning are entirely conveyed from the inferior olive to the cerebellar cortex.

STAR★METHODS

Detailed methods are provided in the online version of this paper and include the following:

- KEY RESOURCES TABLE
- CONTACT FOR REAGENT AND RESOURCE SHARING
- EXPERIMENTAL MODEL AND SUBJECT DETAILS
- METHOD DETAILS
  - Surgical Procedures
  - Two-photon Microscopy and Optogenetics
  - Behavior and Sensory Stimuli
  - Silicon Probe Recording
  - Acute Slice Preparation and Recording
  - Data Analysis
- QUANTIFICATION AND STATISTICAL ANALYSIS

SUPPLEMENTAL INFORMATION

Supplemental Information can be found with this article online at https://doi.org/10.1016/j.neuron.2019.03.010.

ACKNOWLEDGMENTS

We thank Samantha Amat for laboratory assistance, Drs. David Fitzpatrick and Hyungbae Kwon for comments on the manuscript, the GENIE program (Janelia Research Campus, including Drs. Jayaraman, Kerr, Kim, Looger, and Svoboda) for freely providing GCaMP6f to the neuroscience community, Dr. Bito (University of Tokyo) for use of RCaMP2, and Dr. Yizhar (Weizmann Institute of Science) for use of somatically targeted *Gt*ACR2. This work was supported by the Max Planck Society, Germany; the Max Planck Florida Institute for Neuroscience; and National Institutes of Health, United States, grants NS083894 and NS105958 (J.M.C.).

AUTHOR CONTRIBUTIONS

Conceptualization, M.A.G. and J.M.C.; Methodology, M.A.G.; Investigation, M.A.G. and A.B.; Writing, M.A.G. and J.M.C.; Funding Acquisition, J.M.C.

DECLARATION OF INTERESTS

The authors declare no competing interests.

Received: September 21, 2018
Revised: February 7, 2019
Accepted: March 5, 2019
Published: March 27, 2019

REFERENCES

Amat, S.B., Rowan, M.J.M., Gaffield, M.A., Bonnan, A., Kikuchi, C., Taniguchi, H., and Christie, J.M. (2017). Using c-kit to genetically target cerebellar molecular layer interneurons in adult mice. PLoS ONE *12*, e0179347.

Apps, R., and Hawkes, R. (2009). Cerebellar cortical organization: a one-map hypothesis. Nat. Rev. Neurosci. *10*, 670–681.

Armbruster, B.N., Li, X., Pausch, M.H., Herlitze, S., and Roth, B.L. (2007). Evolving the lock to fit the key to create a family of G protein-coupled receptors potently activated by an inert ligand. Proc. Natl. Acad. Sci. USA *104*, 5163–5168.

Barski, J.J., Dethleffsen, K., and Meyer, M. (2000). Cre recombinase expression in cerebellar Purkinje cells. Genesis *28*, 93–98.

Brown, S.T., and Raman, I.M. (2018). Sensorimotor integration and amplification of reflexive whisking by well-timed spiking in the cerebellar corticonuclear circuit. Neuron *99*, 564–575.e2.

Callaway, J.C., Lasser-Ross, N., and Ross, W.N. (1995). IPSPs strongly inhibit climbing fiber-activated [Ca2+]i increases in the dendrites of cerebellar Purkinje neurons. J. Neurosci. *15*, 2777–2787.

Chadderton, P., Margrie, T.W., and Häusser, M. (2004). Integration of quanta in cerebellar granule cells during sensory processing. Nature *428*, 856–860.

Chen, T.W., Wardill, T.J., Sun, Y., Pulver, S.R., Renninger, S.L., Baohan, A., Schreiter, E.R., Kerr, R.A., Orger, M.B., Jayaraman, V., et al. (2013). Ultrasensitive fluorescent proteins for imaging neuronal activity. Nature *499*, 295–300.

Chen, S., Augustine, G.J., and Chadderton, P. (2017). Serial processing of kinematic signals by cerebellar circuitry during voluntary whisking. Nat. Commun. *8*, 232.

Chorev, E., Yarom, Y., and Lampl, I. (2007). Rhythmic episodes of subthreshold membrane potential oscillations in the rat inferior olive nuclei in vivo. J. Neurosci. *27*, 5043–5052.

Coesmans, M., Weber, J.T., De Zeeuw, C.I., and Hansel, C. (2004). Bidirectional parallel fiber plasticity in the cerebellum under climbing fiber control. Neuron *44*, 691–700.

Crill, W.E. (1970). Unitary multiple-spiked responses in cat inferior olive nucleus. J. Neurophysiol. *33*, 199–209.

Davie, J.T., Clark, B.A., and Häusser, M. (2008). The origin of the complex spike in cerebellar Purkinje cells. J. Neurosci. *28*, 7599–7609.

De Gruijl, J.R., Bazzigaluppi, P., de Jeu, M.T., and De Zeeuw, C.I. (2012). Climbing fiber burst size and olivary sub-threshold oscillations in a network setting. PLoS Comput. Biol. *8*, e1002814.

Gaffield, M.A., and Christie, J.M. (2017). Movement rate is encoded and influenced by widespread, coherent activity of cerebellar molecular layer interneurons. J. Neurosci. *37*, 4751–4765.

Gaffield, M.A., Amat, S.B., Bito, H., and Christie, J.M. (2016). Chronic imaging of movement-related Purkinje cell calcium activity in awake behaving mice. J. Neurophysiol. *115*, 413–422.

Gaffield, M.A., Rowan, M.J.M., Amat, S.B., Hirai, H., and Christie, J.M. (2018). Inhibition gates supralinear Ca^{2+} signaling in Purkinje cell dendrites during practiced movements. eLife *7*, e36246.

Govorunova, E.G., Sineshchekov, O.A., Janz, R., Liu, X., and Spudich, J.L. (2015). NEUROSCIENCE. Natural light-gated anion channels: a family of microbial rhodopsins for advanced optogenetics. Science *349*, 647–650.

Hansel, C., and Linden, D.J. (2000). Long-term depression of the cerebellar climbing fiber–Purkinje neuron synapse. Neuron *26*, 473–482.

Herzfeld, D.J., Kojima, Y., Soetedjo, R., and Shadmehr, R. (2018). Encoding of error and learning to correct that error by the Purkinje cells of the cerebellum. Nat. Neurosci. *21*, 736–743.

Hyvärinen, A. (1999). Fast and robust fixed-point algorithms for independent component analysis. IEEE Trans. Neural Netw. *10*, 626–634.

Inoue, M., Takeuchi, A., Horigane, S., Ohkura, M., Gengyo-Ando, K., Fujii, H., Kamijo, S., Takemoto-Kimura, S., Kano, M., Nakai, J., et al. (2015). Rational design of a high-affinity, fast, red calcium indicator R-CaMP2. Nat. Methods *12*, 64–70.

Khosrovani, S., Van Der Giessen, R.S., De Zeeuw, C.I., and De Jeu, M.T. (2007). In vivo mouse inferior olive neurons exhibit heterogeneous

subthreshold oscillations and spiking patterns. Proc. Natl. Acad. Sci. USA *104*, 15911–15916.

Kitamura, K., and Häusser, M. (2011). Dendritic calcium signaling triggered by spontaneous and sensory-evoked climbing fiber input to cerebellar Purkinje cells in vivo. J. Neurosci. *31*, 10847–10858.

Leznik, E., and Llinás, R. (2005). Role of gap junctions in synchronized neuronal oscillations in the inferior olive. J. Neurophysiol. *94*, 2447–2456.

Llinás, R., and Sugimori, M. (1980). Electrophysiological properties of in vitro Purkinje cell dendrites in mammalian cerebellar slices. J. Physiol. *305*, 197–213.

Ly, R., Bouvier, G., Szapiro, G., Prosser, H.M., Randall, A.D., Kano, M., Sakimura, K., Isope, P., Barbour, B., and Feltz, A. (2016). Contribution of post-synaptic T-type calcium channels to parallel fibre-Purkinje cell synaptic responses. J. Physiol. *594*, 915–936.

Maruta, J., Hensbroek, R.A., and Simpson, J.I. (2007). Intraburst and interburst signaling by climbing fibers. J. Neurosci. *27*, 11263–11270.

Matei, V., Pauley, S., Kaing, S., Rowitch, D., Beisel, K.W., Morris, K., Feng, F., Jones, K., Lee, J., and Fritzsch, B. (2005). Smaller inner ear sensory epithelia in Neurog 1 null mice are related to earlier hair cell cycle exit. Dev. Dyn. *234*, 633–650.

Mathy, A., Ho, S.S., Davie, J.T., Duguid, I.C., Clark, B.A., and Häusser, M. (2009). Encoding of oscillations by axonal bursts in inferior olive neurons. Neuron *62*, 388–399.

Najafi, F., and Medina, J.F. (2013). Beyond "all-or-nothing" climbing fibers: graded representation of teaching signals in Purkinje cells. Front. Neural Circuits *7*, 115.

Najafi, F., Giovannucci, A., Wang, S.S., and Medina, J.F. (2014a). Coding of stimulus strength via analog calcium signals in Purkinje cell dendrites of awake mice. eLife *3*, e03663.

Najafi, F., Giovannucci, A., Wang, S.S., and Medina, J.F. (2014b). Sensory-driven enhancement of calcium signals in individual Purkinje cell dendrites of awake mice. Cell Rep. *6*, 792–798.

Nitta, K., Matsuzaki, Y., Konno, A., and Hirai, H. (2017). Minimal Purkinje cell-specific PCP2/L7 promoter virally available for rodents and non-human primates. Mol. Ther. Methods Clin. Dev. *6*, 159–170.

Otsu, Y., Marcaggi, P., Feltz, A., Isope, P., Kollo, M., Nusser, Z., Mathieu, B., Kano, M., Tsujita, M., Sakimura, K., and Dieudonné, S. (2014). Activity-dependent gating of calcium spikes by A-type K+ channels controls climbing fiber signaling in Purkinje cell dendrites. Neuron *84*, 137–151.

Ozden, I., Lee, H.M., Sullivan, M.R., and Wang, S.S. (2008). Identification and clustering of event patterns from in vivo multiphoton optical recordings of neuronal ensembles. J. Neurophysiol. *100*, 495–503.

Piochon, C., Titley, H.K., Simmons, D.H., Grasselli, G., Elgersma, Y., and Hansel, C. (2016). Calcium threshold shift enables frequency-independent control of plasticity by an instructive signal. Proc. Natl. Acad. Sci. USA *113*, 13221–13226.

Rancz, E.A., and Häusser, M. (2006). Dendritic calcium spikes are tunable triggers of cannabinoid release and short-term synaptic plasticity in cerebellar Purkinje neurons. J. Neurosci. *26*, 5428–5437.

Roome, C.J., and Kuhn, B. (2018). Simultaneous dendritic voltage and calcium imaging and somatic recording from Purkinje neurons in awake mice. Nat. Commun. *9*, 3388.

Rowan, M.J.M., Bonnan, A., Zhang, K., Amat, S.B., Kikuchi, C., Taniguchi, H., Augustine, G.J., and Christie, J.M. (2018). Graded control of climbing-fiber-mediated plasticity and learning by inhibition in the cerebellum. Neuron *99*, 999–1015.e6.

Schultz, S.R., Kitamura, K., Post-Uiterweer, A., Krupic, J., and Häusser, M. (2009). Spatial pattern coding of sensory information by climbing fiber-evoked calcium signals in networks of neighboring cerebellar Purkinje cells. J. Neurosci. *29*, 8005–8015.

Tempia, F., Alojado, M.E., Strata, P., and Knöpfel, T. (2001). Characterization of the mGluR(1)-mediated electrical and calcium signaling in Purkinje cells of mouse cerebellar slices. J. Neurophysiol. *86*, 1389–1397.

Vogelstein, J.T., Packer, A.M., Machado, T.A., Sippy, T., Babadi, B., Yuste, R., and Paninski, L. (2010). Fast nonnegative deconvolution for spike train inference from population calcium imaging. J. Neurophysiol. *104*, 3691–3704.

Wang, S.S., Denk, W., and Häusser, M. (2000). Coincidence detection in single dendritic spines mediated by calcium release. Nat. Neurosci. *3*, 1266–1273.

Yang, Y., and Lisberger, S.G. (2014). Purkinje-cell plasticity and cerebellar motor learning are graded by complex-spike duration. Nature *510*, 529–532.

STAR★METHODS

KEY RESOURCES TABLE

REAGENT or RESOURCE	SOURCE	IDENTIFIER
Bacterial and Virus Strains		
AAV1-Pcp2.4-GCaMP6f	Custom Prep (UNC Vector Core)	N/A
AAV1-Pcp2.6-FLPo	Custom Prep (ViGene)	N/A
AAV1-CAG-Flex(*loxP*)rev-GCaMP6f	Penn Vector Core	AV-1-PV2816
AAV1-CAG-Flex(FRT)rev-GCaMP6f	Custom Prep (ViGene)	N/A
AAV1-CAG-Flex(*loxP*)rev-RCaMP2	Custom Prep (Penn Vector Core)	N/A
AAV1-αCaMKII-GCaMP6f	Penn Vector Core	AV-1-PV3435
AAV1-CAG-Flex(*loxP*)rev-ChR2-2a-hM4d	Custom Prep (ViGene)	N/A
AAV1-Syn-GCaMP6f	Penn Vector Core	AV-1-PV2822
AAV1-αCaMKII-GtACR2-eFYP	Custom Prep (ViGene)	N/A
AAV1-αCaMKII-GtACR2-TS-Fred-Kv2.1	Yizhar Lab; https://dx.doi.org/10.1101/225847	N/A
Experimental Models: Organisms/Strains		
Mouse: C57BL/6J	The Jackson Laboratory	Stock #000664; RRID: IMSR_JAX:000664
Mouse: *Kit::Cre*	Amat et al., 2017	Stock #032923; RRID: IMSR_JAX:032923
Mouse: B6.Cg-Tg(Math1-cre)1Bfri/J	The Jackson Laboratory	Stock #011104; RRID: IMSR_JAX:011104
Mouse: B6.129-Tg(Pcp2-cre)2Mpin/J	The Jackson Laboratory	Stock #004146; RRID: IMSR_JAX:004146
Software and Algorithms		
MATLAB	MathWorks; https://www.mathworks.com	RRID: SCR_001622
GraphPad Prism	GraphPad; https://www.graphpad.com	RRID: SCR_002798
Excel	Microsoft; https://www.microsoft.com	RRID: SCR_016137
bControl	Carlos Brody, Princeton; https://brodywiki.princeton.edu/bcontrol/index.php/Main_Page	N/A
ScanImage	Vidrio Technologies; http://scanimage.vidriotechnologies.com	RRID: SCR_014307
pClamp	Molecular Devices; https://www.moleculardevices.com/	RRID: SCR_011323
Fast ICA	Hyvärinen, 1999; research.ics.aalto.fi/ica/fastica/	N/A
Fast oopsi	Vogelstein et al., 2010; https://github.com/jovo/fast-oopsi	N/A

CONTACT FOR REAGENT AND RESOURCE SHARING

Further information and requests for resources and reagents should be directed to and will be fulfilled by the Lead Contact, Jason Christie (jason.christie@mpfi.org).

EXPERIMENTAL MODEL AND SUBJECT DETAILS

Our experiments were conducted under approval of the Institutional Animal Care and Use Committee at the Max Planck Florida Institute for Neuroscience. Adult mice (> 10 weeks of age) of both genders (14 female, 16 male) were used for *in vivo* experiments. We used heterozygous *Kit::Cre* mice (n = 16; Amat et al., 2017), homozygous *Pcp2::Cre* (n = 4; Barski et al., 2000; Jax #004146), heterozygous *Math1::Cre* (n = 6; Matei et al., 2005; Jax #011104), or C57BL/6J mice (n = 4; Jax #000664). For slice experiments, we used C57BL/6J mice (9-10 weeks old, n = 5). All mice were housed in reverse light/dark cycle and received enrichment with running disks.

METHOD DETAILS

Surgical Procedures

Surgeries were performed under isoflurane anesthesia (1.5%–2.0%). Once a deep plane of anesthesia was induced, determined by the lack of response to a toe pinch, a lubricating ointment was applied to the eyes and the animal was injected subcutaneously with carprofen (5 mg/kg), dexamethasone (3 mg/kg), and buprenorphine (0.35 mg/kg) to reduce post-surgical swelling and pain. The hair covering the top of the skull was removed and the exposed skin disinfected with iterative scrubs of iodine and ethanol solutions. Throughout surgery, body temperature was maintained at 37°C using a heating pad with biofeedback control. Topical application of lidocaine/bupivacaine to the surgical site provided local anesthesia. The skin overlaying the skull was excised, and then the skull was gently scraped clean with a scalpel before a custom-made stainless steel head post was attached using dental cement (Metabond; Parkell, Edgewood, NY). A small craniotomy about 2 mm square was cut over left Crus I/II centered approximately 3.5 mm laterally and 2.2 mm caudally from lambda. This craniotomy exposed portions of zebrin bands 7+, 6-, and 6+ of both lobules. Care was taken to avoid damaging the dura.

AAVs, singly or in combination, were injected through a lone, beveled-tip glass micropipette into the exposed brain. We relied on conditional AAVs often in combination with Cre-driver line mice to express genetically encoded Ca^{2+} indicators and activity effectors in a cell-type specific manner. PCs were targeted in *Pcp2::Cre* mice using AAV1-CAG-Flex(*loxP*)rev-GCaMP6f. In *Kit::Cre*, *Math1::Cre*, or C57BL/6J mice, PCs were targeted for transduction using a truncated version of the *Pcp2* promoter (Nitta et al., 2017). Either AAV1-Pcp2.4-GCaMP6f, or AAV1-Pcp2.6-FLPo in combination with AAV1-CAG-Flex(FRT)rev-GCaMP6f. MLIs were targeted in *Kit::Cre* mice using AAV1-CAG-Flex(*loxP*)rev-RCaMP2. For differential targeting of both MLIs and PCs in the same brain region, this RCaMP2-containing AAV was injected in combination with AAV1-Pcp2.6-FLPo and AAV1-CAG-Flex(FRT)rev-GCaMP6f. To express Ca^{2+} indicator in MLIs in *Math1::Cre* mice, we used AAV1-Syn-GCaMP6f. Granule cells were targeted in *Math1::Cre* mice using AAV1-Flex(*loxP*)rev-ChR2-2a-hM4d. A total volume of 250-400 nL of high titer viral particles (e^12–e^13) were pressure injected into the tissue at a rate of ~25 nL/min. Intraperitoneal injections of *D*-mannitol (750 mg/kg) promoted viral spread.

For targeting the inferior olive, viral particles (AAV1-αCaMKII-GCaMP6f, AAV1-αCaMKII-*Gt*ACR2-eFYP or, in one animal, AAV1-αCaMKII-*Gt*ACR2-ST-FRed-Kv2.1 to restrict expression to the soma) were injected into the brainstem (~500 nL; 25 nL/min) at the following coordinates: x = 0.3 mm, y = −4.9 mm, z = −4.6 mm, at a depth of 3.6 mm and an approach angle of 62°. In optogenetic experiments, an optical fiber (CFMLC21U; 105 μm, 0.22 NA, 3.5 mm in length; Thorlabs; Newton, NJ) was then inserted using the same coordinates, and secured in place with dental cement.

After completion of viral injections, a small glass coverslip (CS-3R; Warner Instruments, Hamden, CT) was attached to the skull over the craniotomy using cyanoacrylate glue and then encased with dental cement that also covered any exposed parts of the skull. Care was taken to minimize the amount of pressure exerted by the glass onto the brain's surface. The animals were recovered until ambulatory and monitored for signs of stress and discomfort for 7 days before proceeding to further manipulations.

Two-photon Microscopy and Optogenetics

2pLSM was used for measuring *in vivo* Ca^{2+} activity in neurons of the lateral cerebellum with a custom-built, movable-objective microscope as described previously (Gaffield et al., 2016; Gaffield and Christie, 2017). Video-rate frame scanning (~30 frames/s) at high resolution (512 × 512 pixels) was achieved using an 8 kHz resonant scan mirror in combination with a galvanometer mirror (Cambridge Technologies; Bedford, MA). We used a 16x, 0.8 NA water immersion objective (Olympus; Center Valley, PA) and diluted ultrasound gel (1:10 with distilled water) as an immersion media (Aquasonic; Parker Labs, Fairfield, NJ). The two-channel light-collection pathway, separating green and red light, used high-sensitivity photomultiplier tubes for detection of emitted photons (H10770PA-40, Hamamatsu; Bridgewater, NJ). The microscope was controlled using ScanImage 2015 software (Vidrio Technologies; Ashburn, VA). GCaMP6f (Chen et al., 2013) was excited at 900 nm (Chameleon Vision S, Coherent, Santa Clara, CA). For PCs, we used < 50 mW of power at the objective and ~100 mW for imaging CFs. RCaMP2 (Inoue et al., 2015) was excited at 1070 nm (Fidelity 2, Coherent) with < 60 mW of power.

Optogenetic stimulation of *Gt*ACR2 was driven by 473 nm light from a continuous-wave laser (MBL-F-473-200mW; CNI Optoelectronics; Changchun, China). The laser path included an acousto-optic modulator for precise control of light timing (MTS110-A3-VIS controlled by a MODA110 Fixed Frequency Driver; AA Opto-Electronic; Orsay, France). Laser light was launched into a fiber port (PAF-X-11-A; Thorlabs) and directed into a patch cable (105 mm diameter core, 0.22 NA; M61L01; Thorlabs). This delivered laser light to the optically matched fiber implant. A ceramic connector (ADAL1; Thorlabs), covered with two layers of black shrink tubing and black masking tape, limited escape of stray light and secured the patch cable to the implant. Light out of the end of the patch cable was < 1 mW. Light on conditions lasted 10-30 s for spontaneous activity measurements and 30 s for sensory stimulation experiments.

Behavior and Sensory Stimuli

Mice were head restrained by their surgically attached head post during neural activity monitoring; prior acclimatization allowed familiarity to restraint and improved the stability of recordings. Animals were water restricted (1 mL/day) to associate restraint to reward allocation, a procedure that improved recording stability. All water was provided before beginning any trials.

For sensory stimuli, a pure auditory tone (12 kHz) was generated by a microcontroller (Mega; Arduino; Ivrea, Italy) attached to a speaker positioned on the right side of the animal (~85 dB at the animal's ear). Somatosensory stimulation was achieved using a focused air puff (18 psi; from a compressed nitrogen source), delivered from a needle positioned 3 cm from the face, onto the left whisker pad. A visual stimulus was generated by a 473 nm light source (either a laser or LED), transmitted through the capped end of an optical patch cable (25 μW) visible from the left eye. All stimuli were 150 ms in duration. The same stimulus type was repeatedly delivered (15x) in a block of trials (0.5 Hz). For each block of trials, the modality order was randomized to limit habituation. Stimulus presentation as well as task timing and monitoring were controlled with bControl software (Brody Lab; Princeton).

Optogenetic suppression trials were interleaved with control trials to confirm responsiveness to sensory stimuli. For experiments conducted under anesthesia, ketamine/xylazine (100 and 10 mg/kg, respectively) was delivered by intraperitoneal injection. For experiments using the chemogenetic inhibitor hM4d, CNO was injected via intraperitoneal injection at 5 mg/kg. Experiments were started 45 min after injection. Control measurements from these animals were obtained at least 24 h before and at least 24 h after CNO injection. Importantly, acutely administered CNO does not alter CF-evoked dendritic Ca^{2+} responses in PCs (Gaffield et al., 2018) nor MLI activity (Gaffield and Christie, 2017) indicating the lack of off-target drug effects. Post hoc histology was used to confirm hM4d expression as described previously (Gaffield et al., 2018).

Silicon Probe Recording

To gain access to Crus I, the glass window overlaying the cerebellum was removed along with the dura, both under 1.5% isoflurane anesthesia. Artificial cerebrospinal fluid (142 mM NaCl, 5 mM KCl, 1.3 mM $MgCl_2$, 3.1 mM $CaCl_2$, 10 mM glucose, 10 mM HEPES) was applied to the exposed brain. A grounding silver wire was also cemented to the skull at this time. Recording began in awake animals at least 45 min after recovery from anesthesia. A high-electrode-density silicon probe (H2 type, Cambridge Neurotech; Cambridge, England) was slowly lowered into Crus I using a micromanipulator until activity was observed. The probe was attached to an RHD2132 amplifier board connected to an RHD2000 series recording controller both from Intan Technologies (Los Angeles, CA). Data were sampled at 20 kHz. This interfaced with Recording Controller Software (Intan Technologies).

Acute Slice Preparation and Recording

Under ketamine/xylazine anesthesia (intraperitoneal injection; 20mg/mL; 2mg/mL respectively), mice were transcardially perfused with cold saline (~4°C) to rapidly chill the brain and the cerebellum was then removed by dissection. Slices (200 μm) were sectioned in the parasagittal orientation from the lateral cortical hemisphere using a vibrating blade microtome (VT1200S, Leica Biosystems, Wetzlar, Germany) in an icy solution containing (in mM) 87 NaCl, 25 $NaHCO_3$, 2.5 KCl, 1.25 NaH_2PO_4, 7 $MgCl_2$, 0.5 $CaCl_2$, 10 glucose, and 75 sucrose. Slices were transferred to an incubation chamber containing a similar solution but with (in mM) 128 NaCl, 26.2 $NaHO_3$, 2.5 KCl, 1 NaH_2PO_4, 1.5 $CaCl_2$, 1.5$MgCl_2$ and 11 glucose and maintained at 34°C for 30 min and then at room temperature (23-25°C) thereafter. During whole-cell recording, slices were continuously perfused with the same solution warmed to 32°C with an inline heater (TC-344; Warner Instruments). All solutions were equilibrated and maintained with carbogen gas (95% O_2/5% CO_2).

PCs in Crus I/II were targeted for somatic whole-cell recording using gradient-contrast video-microscopy and recorded using borosilicate patch pipettes containing an intracellular solution composed of (in mM) 128 potassium gluconate, 2 KCl, 9 HEPES, 4 $MgCl_2$, 4 NaATP, and 0.5 NaGTP (pH = 7.25). Open tip resistance was 2-4 MΩ. During whole-cell recording, constant current injection maintained the membrane potential of PCs at ~-60 mV. Electrophysiological measurements were obtained using Multiclamp 700B amplifiers (Molecular Devices, San Jose, CA). Analog signals were filtered at 4 kHz and sampled at 50 kHz using a Digidata 1440 digitizer (Molecular Devices). Data were collected using pClamp 10 software (Molecular Devices). Pipette capacitance was neutralized in all recordings and electrode series resistance compensated using bridge balance in current-clamp mode. Brief electrical pulses (100 μs; 0.5 – 2.0 V) applied through a constant voltage stimulus isolation unit (Model DS2A; Digitimer, Ft. Lauderdale, FL) were used to activate CFs with bi-polar glass pipettes placed near the PC soma.

PCs were filled through the whole-cell pipette with the green Ca^{2+} indicator Fluo-5F (200 μM; Invitrogen, Carlsbad, CA) as well as the red-volume indicator Alexa 594 (20 μM; Invitrogen) to identify their dendritic processes. PCs were imaged with 2pLSM. The microscope consisted of a commercial scan head (Ultima; Bruker Corp, Billerica, MA) fitted with galvanometer mirrors (Cambridge Technologies) that sat on an Olympus upright microscope (BX51WI) using an objective (20x, 1.0 NA) and oil immersion condenser (1.4 NA). Single wavelength 2p excitation (λ = 810 nm) was provided by a mode-locking Ti:sapphire laser (Chameleon Ultra II; Coherent). Fluorescence emission was detected using GaAsP photomultiplier modules (Hamamatsu) with a t560lpxr dichroic and et640/120-2p and et510/80-2p bandpass filters (Chroma, Bellows Falls, VT) for chromatic separation. Ca^{2+} activity measurements were obtained in frame-scan mode (~24 frames/s) over branched dendritic regions (10 × 10 μm) simultaneous with the somatic electrophysiological response during CF stimulation.

Data Analysis

All data were analyzed using custom-written routines in MATLAB (MathWorks; Natick, MA). Time-series images of Ca^{2+} activity in neurons expressing genetically encoded Ca^{2+} indicators were aligned using a least-squares algorithm. PCs and CFs were segmented using an independent component analysis algorithm to group like-responding pixels (Hyvärinen, 1999) and Ca^{2+} events identified using an inference-based method (Gaffield et al., 2016; Vogelstein et al., 2010). The effective Ca^{2+} event rate during a trial

was calculated from the probability of an event occurring in each frame (34 ms in duration) across all segmented PCs and CFs in the field of view. For CFs, event rate reflects the number of discrete bursts, as each burst is registered as an individual event, because discriminating each spike in a burst - expected to be > 250 Hz (Mathy et al., 2009) - is well beyond the temporal resolution of our detection system.

For analysis of Ca^{2+} event size, we focused on discrete, isolated responses (Gaffield et al., 2018). Thus, we avoided potential uncertainties associated with GCaMP6f non-linearity (Chen et al., 2013) for overlapping events. For inclusion, events must have been separated by at least 500 ms from proceeding or following events for PCs and 300 ms for CFs, a time window allowing for a nearly complete decay of the response. Events were categorized as sensory-related if they occurred within 250 ms of stimulus onset. Events outside of this window were categorized as spontaneous. ΔF/F was calculated using a baseline fluorescence period immediately prior to an identified event (200 ms). To quantify event size, we measured the peak of the integral of the Ca^{2+} response, a metric identical to previous reports (Najafi et al., 2014a, 2014b). For this, we first calculated the ΔF/F for all identified, isolated spontaneous and sensory-related events measured during a block of trials for PCs in a field of view. These averaged responses were then integrated over a time interval beginning at the peak ΔF and ending 100 ms later. The peak amplitudes of the integrals were normalized to the spontaneous response facilitating averaging across sensory modalities, fields of view, and measurements from different mice.

For trial-averaged PC Ca^{2+} activity measurements that were irrespective of isolated events, we simply calculated ΔF/F for all PC dendrite regions of interest (ROIs) and aligned responses to the onset of the sensory stimulus. In a subset of curated trials, we removed putative CF-evoked events from response averages similar to a previous report (Najafi et al., 2014b). However, in our approach, we used an inference algorithm (Vogelstein et al., 2010) rather than template matching to identify putative CF-evoked events in PC dendrites. Fluorescence from any trials that resulted in no event was then integrated over the time period beginning two frames after the stimulus and ending 100 ms later. This value was then compared to the integral distribution for all spontaneous events. Any trial with a value within this distribution was also defined as CF-evoked and removed from the average. Fluorescence from the remaining trials was then averaged to produce a "non-CF" trace (Figure S6). For *ex vivo* recordings, CF-evoked Ca^{2+} signals were quantified as the change in green fluorescence from the Ca^{2+} indicator normalized to red fluorescence from the volume indicator (ΔG/R).

MLI ROIs were hand-drawn from time-averaged images; automated segmentation was difficult because MLIs respond in a nearly identical manner (Gaffield and Christie, 2017). Therefore, for population analysis, we used an ROI encompassing large regions within the field of view to measure and quantify sensory-evoked Ca^{2+} activity. For dual-color Ca^{2+} imaging, epochs of spontaneous MLI activity were temporally registered to that of CF-evoked Ca^{2+} events in PCs; a mask comprising all pixels corresponding to MLIs within 50 μm of each PC was used to calculate the time-locked average of MLI activity during these periods.

In *in vivo* extracellular electrophysiology recordings, PC units were first identified post hoc based on evidence of clear complex spikes. Once all channels with PCs were identified, we sorted out unique cells based on autocorrelations with a clear refractory period > 5 ms between events and cross-correlations across units with no peak at 0 time lag. Only PC units that had a complete absence of complex spikes during optogenetic suppression of the inferior olive were used in the analysis. Complex and simple spikes were identified using a thresholding algorithm.

QUANTIFICATION AND STATISTICAL ANALYSIS

Additional calculations, statistical analysis, and plotting was performed in either Excel (Microsoft, Redmond, WA) or Prism (GraphPad, La Jolla, CA). Significance was defined as having a p value < 0.05. Student's t tests and ANOVAs were used where appropriate as indicated in the text. In figures, neural activity traces are shown with the mean response in bold and ± SEM in the shaded region. In summary plots, data are represented as mean with error bars indicating SEM. We did not perform a power analysis prior to experiments to estimate replicate numbers.